



HAL
open science

Physical modelling of an array of 25 heaving wave energy converters to quantify variation of response and wave conditions

Peter Troch, Vasiliki Stratigaki, Tim Stallard, David Forehand, Matt Folley, Jens-Peter Kofoed, Michel Benoit, Aurélien Babarit, David Gallach-Sánchez, Lieselot de Bosscher, et al.

► To cite this version:

Peter Troch, Vasiliki Stratigaki, Tim Stallard, David Forehand, Matt Folley, et al.. Physical modelling of an array of 25 heaving wave energy converters to quantify variation of response and wave conditions. 10th European Wave and Tidal Energy Conference (EWTEC2013), Sep 2013, Aalborg, Denmark. hal-01201906

HAL Id: hal-01201906

<https://hal.science/hal-01201906v1>

Submitted on 14 Jul 2019

HAL is a multi-disciplinary open access archive for the deposit and dissemination of scientific research documents, whether they are published or not. The documents may come from teaching and research institutions in France or abroad, or from public or private research centers.

L'archive ouverte pluridisciplinaire **HAL**, est destinée au dépôt et à la diffusion de documents scientifiques de niveau recherche, publiés ou non, émanant des établissements d'enseignement et de recherche français ou étrangers, des laboratoires publics ou privés.

Physical Modelling of an Array of 25 Heaving Wave Energy Converters to Quantify Variation of Response and Wave Conditions

P. Troch^{1*}, V. Stratigaki¹, T. Stallard², D. Forehand³, M. Folley⁴, J.P. Kofoed⁵, M. Benoit⁶, A. Babarit⁷, D. Gallach Sánchez¹, L. De Bosscher¹, P. Rauwoens¹, B. Elsässer⁴, P. Lamont-Kane⁴, P. McCallum³, C. McNatt³, E. Angelelli⁵, A. Percher⁵, E. Carpentero Moreno², S. Bellew², E. Dombre⁶, F. Charrayre⁶, M. Vantorre¹, J. Kirkegaard⁸, S. Carstensen⁸

¹*Ghent University, Belgium, *Peter.Troch@UGent.be*

²*School of Mechanical, Aerospace and Civil Engineering, University of Manchester, UK*

³*Institute for Energy Systems, University of Edinburgh, UK*

⁴*Queens University Belfast, Northern Ireland*

⁵*Aalborg University, Denmark*

⁶*Laboratoire Saint Venant, EDF R&D, Chatou, France*

⁷*Ecole Centrales de Nantes, France*

⁸*DHI, Denmark*

Abstract— Experiments have been performed in the Shallow Water Wave Basin of DHI, in Denmark, on large arrays of up to 25 heaving point absorbers for a range of layout configurations and wave conditions. Float response and modification of the wave field are measured to provide data suitable for the evaluation of array interaction models and environmental scale models. Each wave energy converter unit has a diameter of 0.315 m and power absorption is due to friction of both a power take off system and bearings. Response is measured on all floats and surge force on five floats. Wave gauges are located within and around the array. Wave conditions studied include regular waves and both long- and short-crested irregular waves. A rectilinear arrangement of support structures is employed such that several float configurations can be studied. A summary is presented of the experimental arrangement with particular emphasis on the individual wave energy converters and wave conditions employed. Reasonable agreement is observed between measured response for single floats and power output and float response predicted using a linear time domain model. For an array of 25 floats, up to 16.3% reduction of significant wave height is observed down-wave and 10.8% increase observed up-wave for unidirectional irregular waves due to wave radiation by the heaving WECs. Spectra at different locations within and around the array show the wave field modifications.

Keywords— Array, Wave Energy Converters, Wave Energy, Shallow Water Wave Basin DHI, Point Absorber, Experiment, HYDRALAB IV

I. INTRODUCTION

Several numerical methods have been employed to analyse the response of arrays of wave energy converters (WECs) to the incident wave climate and the modification of wave conditions, particularly down-wave, of such arrays. Reviews of available modelling approaches and their applications are available [1], [2]. Boundary element methods based on potential flow models have been widely used to study the influence of hydrodynamic interactions on float response [3].

One limitation of such methods is that viscous effects are not directly modeled. However, such effects may be parameterized and used particularly in the context of a time-domain simulation. In [4] the application of WAMIT (BEM) and a Navier-Stokes solver has been compared, to identify physics that are not captured by BEM solvers; specifically the vortex shedding around a heaving buoy, wave overtopping, and the re-entering impact of an out-of-water body.

Spectral wave propagation models such as SWAN [5] and MIKE21 [6] have both been employed to study the change of wave conditions inshore of WEC arrays [7]. Representation of large arrays within spectral models may be by transmission and reflection coefficients [8] or subgrid models [9]. The wave-field in the lee of a single WEC and multiple WECs is typically a region of reduced wave energy density and is referred to herein as a wake (referring to the “bow” wake that is created in incompressible fluids such as water, due to waves and not by wind). Wakes have been studied using the mild-slope wave propagation model MILDwave [10]-[12], in which WECs are represented using a sponge layer technique.

In contrast to the large quantity of numerical simulations of WEC arrays and the large body of experimental work concerning individual WECs or pair of WECs [13], [14], there is limited published data concerning either the response of such devices located in arrays or of the corresponding wave-field changes. In the last decade, experimental measurements of the response of the Wave Star WEC - composed of a large number of floating bodies at close proximity and supported by a single structure - have been conducted and have led to construction and testing of a prototype at an offshore site near the Hanstholm location, in Denmark [15]. Experimental studies of arrays of 5 and 12 closely spaced heaving floats have also been conducted including response to regular waves [16], power output and response in irregular waves [17] and wave spectra changes across the array [8]. Within the UK

Supergen Marine and the EU Hydralab III programmes, tests have been conducted of a WEC array of five oscillating water columns interconnected by mooring lines [18]. As part of the PerAWaT project several studies of wave energy converter arrays have been conducted, both of idealized geometries (e.g. [19]) and scale models of WEC systems under development by private companies.

Presently, no experimental studies are publicly available detailing wave device response and power output as well as wave field modifications. Such data is essential for evaluation of the accuracy of the previously mentioned numerical tools. Accurate measurement of individual WEC (float) response, WEC array power output and spatial variation of wave conditions in the vicinity of the array are required to improve

understanding of the fundamental processes influencing wave conditions down- and up-wave of wave energy converter arrays. The experiments of Table I have been conducted at DHI within the EU FP7 funded WECwakes project during Quarter 1 2013. An overview of the design and conduct of the experiments is given in Section II. Preliminary analysis of float response and power output is given in Section III with comparison to predictions based on linear hydrodynamics. Changes of significant wave height and wave spectra in the vicinity of a rectilinear array of 25 floats at 5D centre-to-centre spacing is presented in Section IV. A brief discussion on the findings to-date and the use of this data for evaluation of numerical models of wave field changes due to WEC arrays is given in Section V.

TABLE I: WEC CONFIGURATIONS AND WAVE CONDITIONS STUDIED

Configuration	Types of tests					Layout sketch
	Regular	Irregular Long-crested	Irregular Short-crested	Scattered	Decay	
Waves	x	x	x	x (axes)	N/A	
Single WEC	x	x	x	x	x	
2 WEC Column	x	x	x (spacing 5D)	x (spacing 5D)	x	
2 WEC Row	x	x	-	x (spacing 5D)	-	
5 WEC Column	x	x	x (middle column)	x (middle column)	x (middle column)	
5 WEC Row	x	x	-	-	-	
10 WEC Column	x	x	-	-	-	
5x5 WEC Square	x	x	x	x	-	
5x5 WEC offset	x	x	x	x	-	
3x3 square 10D	x	x	x	-	-	
3x3 square 5D	x	x	x	-	-	
13 staggered WECs	x	x	x	x	-	

II. ARRAY EXPERIMENTS

The objective of this study is to measure the wave field in the vicinity of arrays of wave energy converters. The experimental arrangement is selected to attain float response amplitude operator (RAO) greater than unity, and a measurable power output, whilst ensuring that the system is simple to setup for multiple units. A single WEC unit has been developed and characterised through trials in several flumes and basins [20].

A. Wave Energy Converter (WEC)

Each WEC comprises three main parts: (i) a hemispherical ended buoy of diameter, D , and draft, d_{buoy} , 31.5 cm and overall height 60.0 cm, (ii) a vertical steel shaft of 40 mm square section with a gravity base, and (iii) a PTO-system comprising PTFE blocks and 4 linear springs (Fig. 1). The dry mass of the float is $m = 20.545$ kg and natural period, by decay test and response measurement in regular waves, is $T_n = 1.176$ s. The upper part of the buoy is a horizontal PVC cover, on which the PTO-system is installed and a potentiometer is connected (Fig. 1).

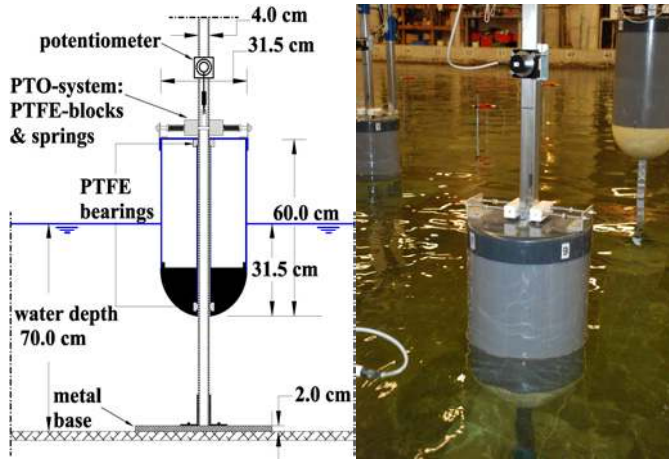


Fig. 1: Cross section of single wave energy device illustrating geometry, bearings and power take off system (left) and image of single unit within array (right).

A power take off force is applied to the buoy by friction brakes (composed of PTFE-blocks and springs) between the float and the supporting axis. The resultant PTO force, F_{PTO} , can be modelled to a reasonable accuracy by Coulomb damping [21] as:

$$F_{PTO}(t) = -\mu F_N \text{sign}(\dot{z}(t)). \quad (1)$$

where μ is the coefficient of friction, F_N is the normal force developed by the brakes and $z(t)$ is the time varying heave displacement of the buoy. In addition to the PTO force, there is also the frictional force, $F_{bearing}$, due to the shaft bearings that are formed using the same PTFE material as the PTO brake. This force is also modelled by Coulomb damping but this time the normal force is taken to be the absolute value of the surge force, F_{surge} :

$$F_{bearing}(t) = -\mu \text{abs}(F_{surge}(t)) \text{sign}(\dot{z}(t)). \quad (2)$$

Net power absorption, P_{tot} , is therefore obtained as:

$$P_{tot}(t) = -\dot{z}(t)(F_{PTO}(t) + F_{bearing}(t)). \quad (3)$$

Since surge force is out of phase with float velocity, power varies substantially during each wave cycle (Fig. 2).

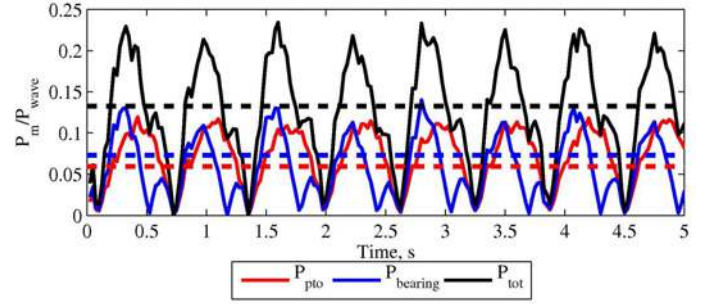


Fig. 2: Typical measured time-variation of power due to constant force power take off (PTO) and time-varying force due to surge force on the bearings.

B. Experiment Configuration

Tests were conducted in the Danish Hydraulics Institute (DHI), Shallow Water Basin. The basin dimensions are 35.0 m x 25.0 m (width x length). 44 wave paddles, each of width 0.5 m are used. The paddles are arranged in two segments of length 16.0 and 6.0 m with a 20.0 cm step between the two segments. Down-wave an absorbing beach with slope of approx. 1/5.59 has been formed using gravel material. In Fig. 3 the stencil configuration comprising 5 x 5 rectilinear WEC array of support structures at centre-to-centre spacing of $5D = 1.575$ m (where D , is the WEC diameter) and the locations of the wave gauges are presented.

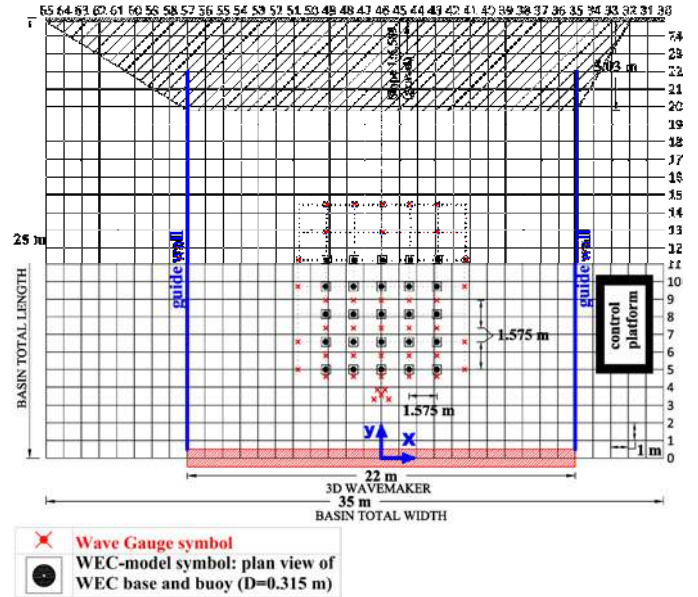


Fig. 3: Arrangement of DHI wave basin and 5 x 5 float stencil. Grid at 1.0 m increments, standard wave gauge arrangement (x) and float positions (•) are indicated. The hatched region along x-axis denotes the extent of the wave paddles. Side walls are plywood guides. Water depth is constant 0.7 m.

The 3D wavemaker in the Shallow water DHI wave basin has a total length of 22.0 m and thus, does not extend across the entire basin width of 35.0 m. Vertical guide walls were installed in order to avoid diffraction of the generated waves to either side of the basin. This technique results to a larger “effective” domain within the wave basin. Moreover, it simplifies the numerical treatment of the experimental set-up (using fully reflective boundaries). The guide walls are nearly 25 diameters from the outermost floats of the 5 x 5 array and so reflection of waves scattered and radiated by the array is not expected to substantially influence the findings. The guide walls comprise plywood panels that extend 2.0 m beyond the toe of the absorbing beach, such that directional waves are not reflected back to the test region.

C. Wave Conditions

Three types of wave have been considered:

- 1) Regular waves,
- 2) Long-crested irregular waves,
- 3) Short-crested irregular waves.

Regular waves are defined in terms of wave period, T , and a wave height, $H = 0.074$ m is employed throughout the tests. Irregular waves are defined by a JONSWAP spectrum with peak period, $T_p = T$, and $H_{m0} = 0.104$ m to achieve equivalent energy density to the regular waves. Directionally spread irregular waves are also considered and defined by a cosine power 2s model [22] with $s = 75$ and $s = 10$ to represent swell and wind seas respectively [23]. For the majority of the tests, two wave periods are considered: $T = T_p = 1.18$ s, coincident with the natural period of the float, T_n , and $T = T_p = 1.26$ s. The water depth, d , has been kept constant throughout the entire testing period at 0.7 m.

For all data reported here, the DHI wave paddles were operated in absorption mode. To determine the incident wave conditions, each sea state has been recorded for three geometric configurations:

- 1) at wave gauge locations used during float tests (WEC units are held stationary above the water surface),
- 2) at wave gauge locations used during float tests without float axes installed (i.e. empty basin),
- 3) at the locations of the float axes (empty basin).

The effect of the presence of the support structures (axes of 40mm x 40mm section) on wave amplitude is confirmed to be small.

For a given distance from the wave-paddles, a variation of wave height is observed across the width of the flume. For regular waves, there is only 3% variation of amplitude between repetition of the same regular wave conditions (Fig. 4) but larger wave heights are observed at $X < -5D$ than $X > +5D$. For irregular waves, the measured height also varies with position within the basin (Figs. 6, 7) although the spatial variation is less than for regular waves. The cause of this spatial variation of height is not entirely clear but it may be due to small differences of wave generation across the flume width and development of reflections from the beach and transverse walls.

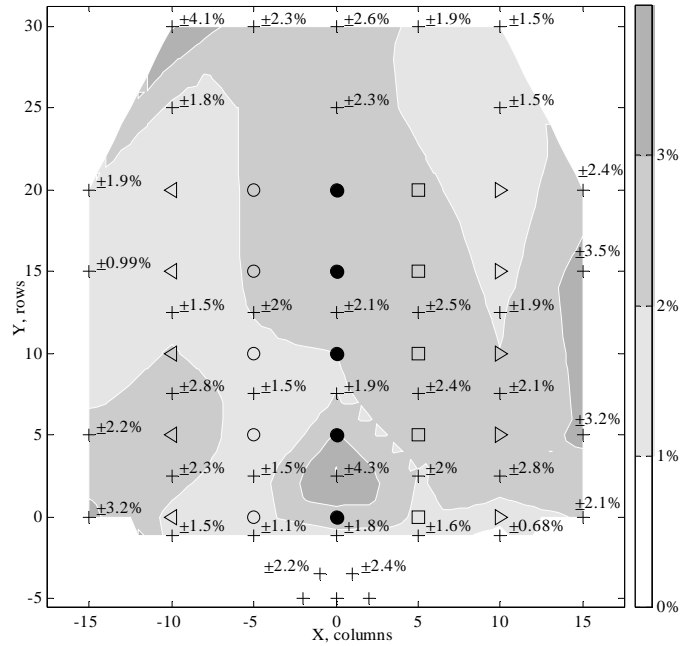


Fig. 4: Standard deviation of the mean of the wave amplitude (a_m/a_0) over eight measurements of the mean amplitude (a_m) of regular waves with target wave amplitude $a_0 = 0.037$ m and wave period $T = 1.26$ s. Shading in contour plot denotes less than 1.0 % (white), 1.0-2.0% (light gray), 2.0-3.0% (gray), >3.0% (dark gray).

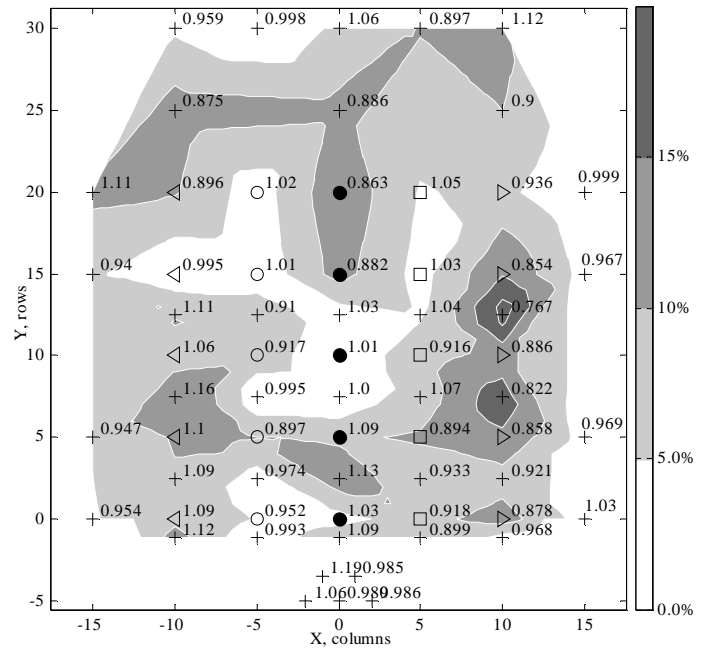


Fig. 5: Variation of measured regular non-dimensional wave amplitude (a_m/a_0) across the test region of the basin for target wave amplitude $a_0 = 0.037$ m and wave period $T = 1.26$ s. Measurements shown at the standard wave gauge locations within and around the array (+) and at the float centerlines (open and solid markers). Data at wave gauge locations recorded with float support axes in position. Data from mean of eight repetitions of wave conditions. Shading in contour plot denotes difference percentage between a_m and a_0 less than 5 % (white), 5-10% (light gray), 10-15% (gray), >15% (dark gray).

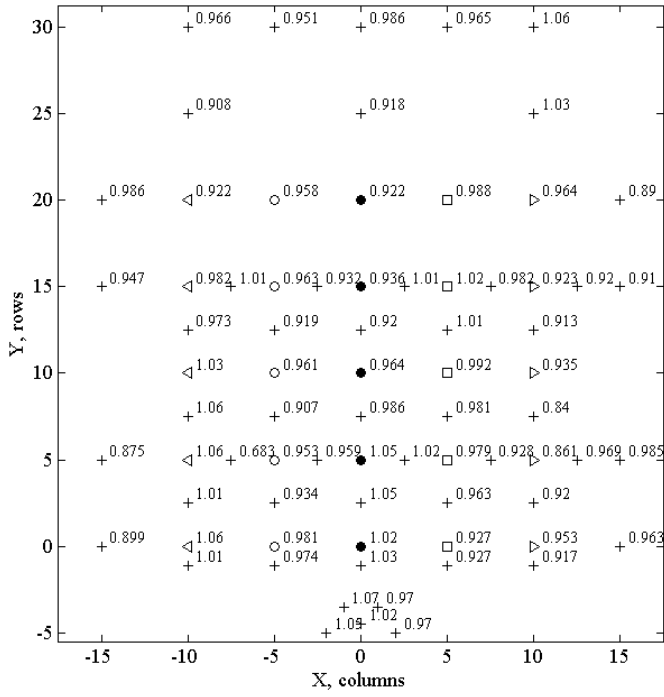


Fig. 6: Variation of non-dimensional significant wave height across the test region of the basin for target conditions of unidirectional waves defined by JONSWAP spectra with $H_{m0} = 0.104$ m, $T_p = 1.26$ s. Measurements shown at the standard wave gauge locations within and around the array (+) and at the float centrelines (open and solid markers). The data at wave gauge locations have been recorded without float axes installed. Data from mean of eight repetitions of wave conditions.

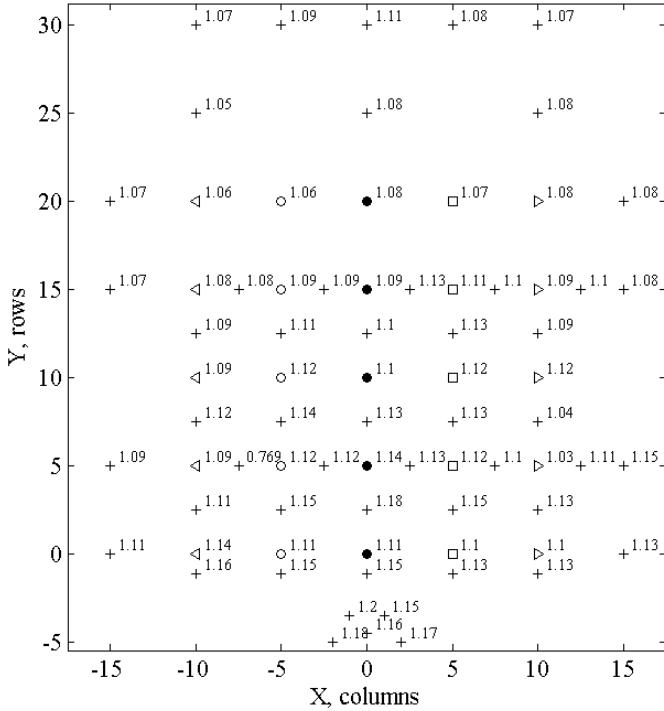
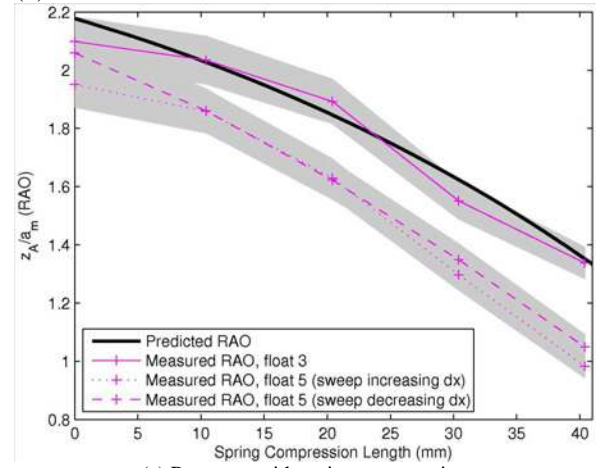


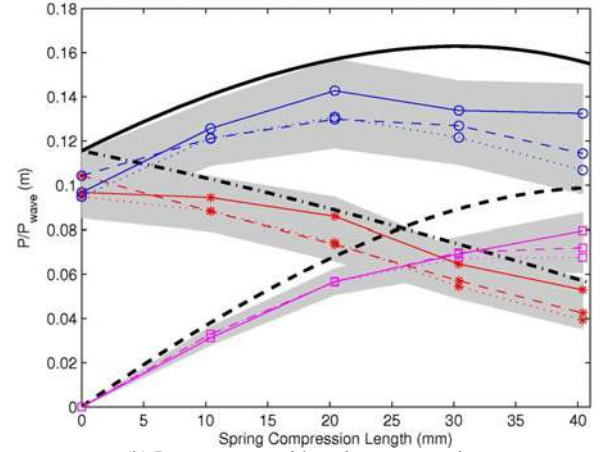
Fig. 7: Variation of non-dimensional significant wave height across the test region of the basin for target conditions of spread irregular waves defined by JONSWAP spectra with $H_{m0} = 0.104$ m, $T_p = 1.26$ s and $s = 10$. The data at wave gauge locations have been recorded without float axes installed. Data from mean of eight repetitions of wave conditions.

III. FLOAT RESPONSE AND POWER OUTPUT

Float response is measured during all tests. Since power absorption is due to a constant spring force and time-varying surge force, response is analysed employing a time-domain model. The approach used follows [24] and is based on hydrodynamic coefficients obtained from the linear frequency-domain code WAMIT [25]. Frequency dependent radiation damping and added mass are subsequently converted, via approximating transfer functions, to a state-space formulation to represent the time-varying hydrodynamic damping force. Both the heave and surge excitation force are also obtained from WAMIT. Hydrodynamic parameters are obtained for a hemispherical ended float only neglecting the support structure arrangement. The mechanical constraints due to PTO and bearing friction are modelled by Equation (1) and (2).



(a) Response with spring compression



(b) Power output with spring compression

Fig. 8: Response and power output with spring compression, dx , from 3 experiments on single float and from numerical prediction. Response graph described by legend and shaded regions indicate $\pm 4\%$ variation in measured amplitudes over three repeats of experiment. For power graph: thick dashed line – predicted PTO power; thick dash-dot line – predicted bearing power; thick solid line – predicted total power; thin magenta lines with squares – measured PTO power; thin red lines with asterisks – measured bearing power; thin blue lines with circles – measured total power; thin solid lines – float 3; thin dotted lines – float 5, sweep increasing dx ; thin dashed lines – float 5, sweep decreasing dx . Shaded regions indicate $\pm 10\%$ variation in measured powers. P_{wave} is the power in the incident wave per metre width (i.e. per unit wavefront).

A coefficient of friction $\mu = 0.17$ is found to provide reasonable agreement between measurement and prediction of response amplitude and mean power absorption over a range of PTO spring compression increments, dx (Figure 8). This coefficient is representative of the friction between PTFE and industrial (non highly polished) steel sliding interfaces [26]. Predicted response is in good agreement with response of one float (float 3) but consistently over predicts that of the second float (float 5). The predicted powers in Fig. 8(b) also show good agreement with the measurements but again there is some discrepancy between the two floats considered. Note that, for this comparison, measured response amplitudes (z_m) are normalised to the wave amplitude measured at the float axes location (a_m) because wave amplitude varies with location within the basin. Power absorption of a float within an array is expected to vary due to float velocity and surge force. For all multi-float tests, the same PTO force is applied to each float for the test duration. For the majority of tests, a spring compression $dx = 30.4$ mm is employed since this corresponds to maximum power absorption as shown in Fig. 8.

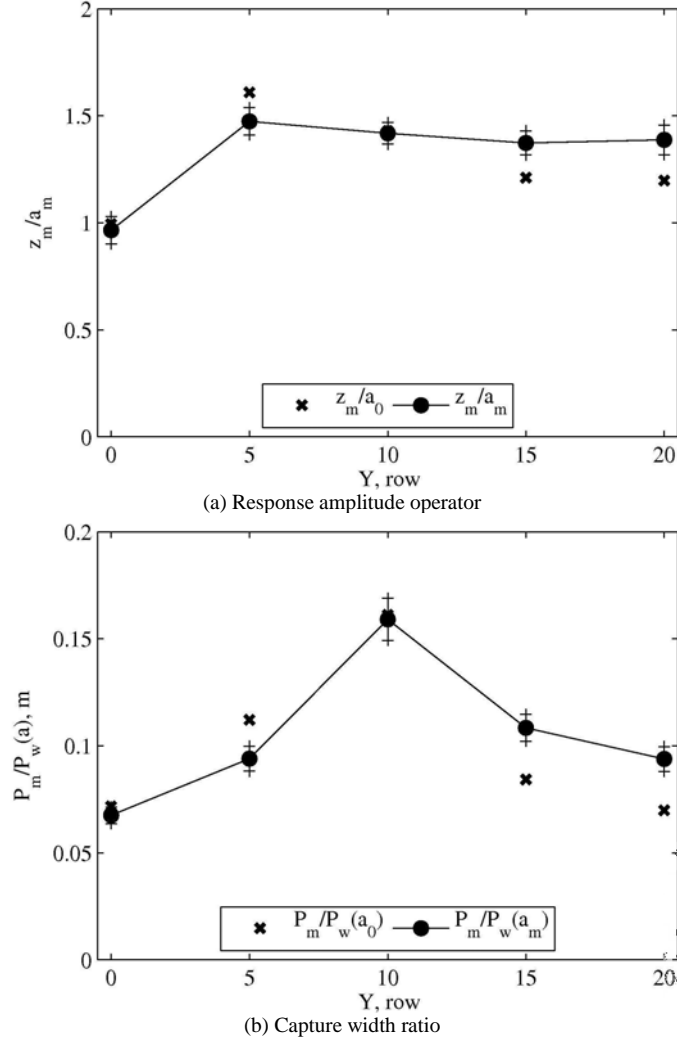


Fig. 9: Response and capture width of five floats at 5D spacing aligned with the wave direction and averaged over 60 wave periods, T. Each is point normalised to measured wave amplitude at float axes (a_m) and target amplitude ($a_0 = 0.037$ m). Error bars denote standard deviation.

Initial analysis of the response of a column of five floats indicates that there is greater variation of absorbed power with position than variation of response with position (Fig. 9). Compared to an isolated float, the response of the front float is reduced and response of float numbers two through to five are comparable. However, the proportion of the incident power absorbed differs by a factor of 2.25 between the front float (at $Y = 0D$) and middle float (at spacing $10D$ from the front float). This spatial variation is greater than both the range of responses observed during the test and the spatial variation of wave amplitude.

IV. WAVE FIELD MODIFICATION

One of the WECwakes project objectives is to study the effect of the WEC array configurations on the wave field. Therefore, the wave field modifications due to wave energy extraction and the WECs' motion have been quantified.

Unidirectional irregular waves are analysed to separate the following contributing wave field components: the scattered wave-field due to the stationary floats and the radiated wave field due to oscillation of the floats. To measure the combined incident and scattered wave, all 25 WEC units are held stationary at mean draft, d_{buoy} . To measure the combined incident, scattered and radiated wave field (the total wave field due to the response of the WECs), damping has been applied through the PTO-system, with $dx = 30.4$ mm spring compression used on each float, and through the shaft bearings. The scattered wave field is then calculated as the difference between the wave measured around fixed floats and the incident wave. The radiated wave field is then calculated as the difference between the measured combined scattered and radiated wave field and the scattered wave field. The radiated wave field includes radiated waves that are subsequently scattered, and it also accounts for the absorption effects at the WECs.

The following difference percentage (x100%) terms are defined and plotted in Fig.10 for an array of 25 WECs:

(a) wave diffraction (scattering around fixed WECs). For quantifying the diffraction effect, the recorded undisturbed wave field when no WECs or axes are present is used to exclude the wave basin effects that develop in the basin without floats installed:

$$\frac{\text{scattered wave field} - \text{recorded undisturbed wave field}}{\text{recorded undisturbed wave field}} \times 100\% \quad (4)$$

(b) a variant of Eq. (4) showing the difference percentage used for quantifying the effect of the wave diffraction (scattering around fixed WECs) relative to the target wave field. This variant shows the differences between the recorded and the target undisturbed wave field when no WECs or axes are present:

$$\frac{\text{scattered wave field} - \text{recorded undisturbed wave field}}{\text{target undisturbed wave field}} \times 100\% \quad (5)$$

(b) difference percentage used for quantifying the effect of radiation due to damped response of 25 WECs on the combined scattered and radiated (total) wave field:

$$\frac{\text{total wave field} - \text{scattered wave field}}{\text{recorded undisturbed wave field}} \times 100\% \quad (6)$$

The data have been analysed using Wavelab [27]. The measured change of the wave field is presented separately for the scattered waves and for the radiated waves for unidirectional irregular waves in Figures 10 (a)-(c). Note that the difference percentages are positive, when scattering effects increase the incident wave field height compared to the incident wave (Figs.10(a) and 10(b)), and when radiation effects increase the total incident wave field height compared to the combined incident and scattered wave field (Fig.10(c)). Negative difference percentages indicate a decrease of the scattered wave field component (Figs.10(a) and 10(b)) and that radiation effects decrease the total incident wave field height (Fig.10(c)).

For an array of 25 aligned floats and unidirectional waves of $T_p = 1.26 \text{ s}$ and $H_{m0} = 0.104 \text{ m}$, up to 5.1 % of wave height decrease downwave and 26.2% wave height increase upwave is observed when the 25 WECs are held stationary at mean draft, d_{buoy} (Fig. 10(a)). These percentages differ slightly in Fig. 10(b) where the recorded wave heights are normalized by the target wave field (5.38 % of wave height decrease downwave and 24.0% wave height increase upwave, respectively). When looking at the effect of the WECs on the wave field due to radiation only (Fig. 10(b)), approximately 16.3% wave height decrease is observed downwave of the array, and 8.75-10.8 % increase upwave.

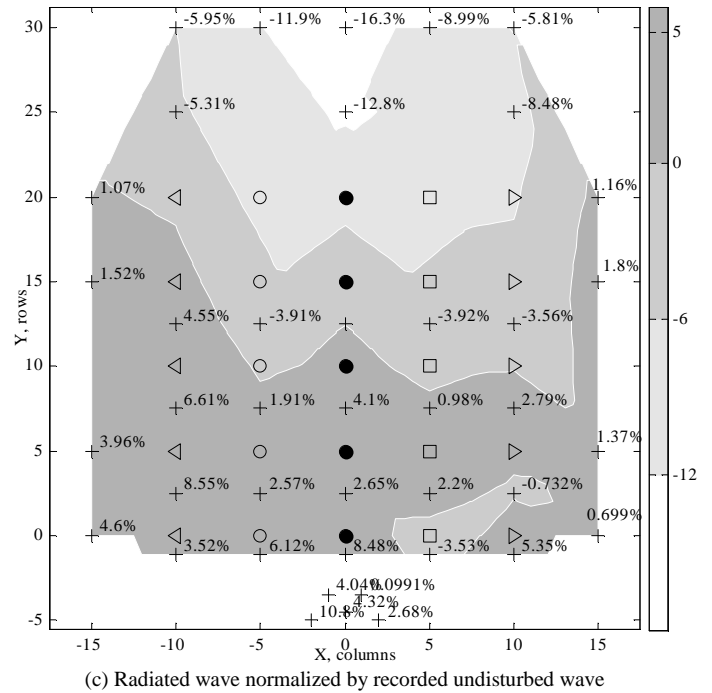
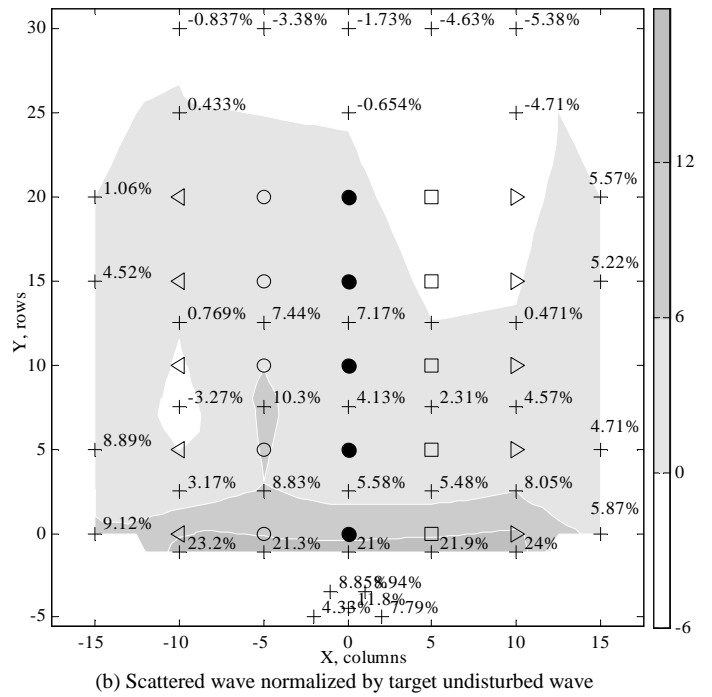
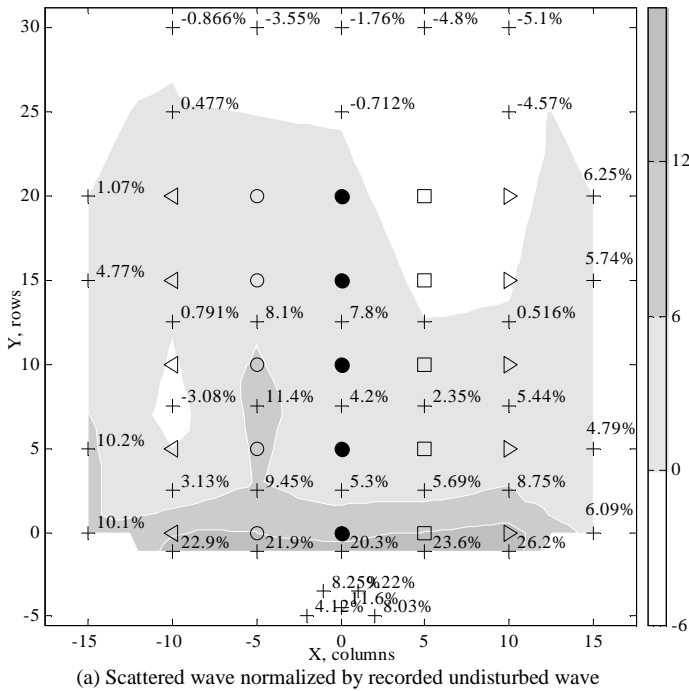
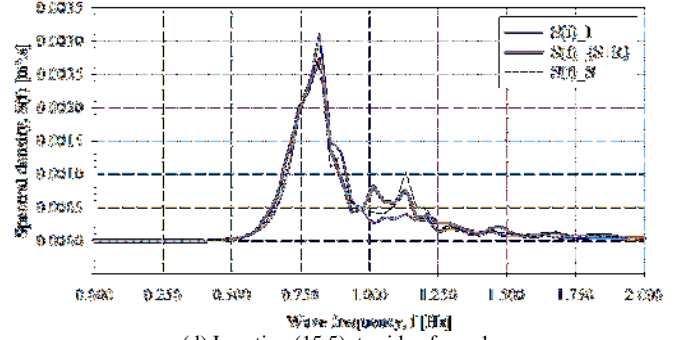


Fig. 10: Non-dimensional percentage (x100%) of change of H_{m0} at locations within and around array of 5 x 5 floats on rectilinear array due to scattered wave (fixed floats) and radiated wave (responding floats with damping applied). Unidirectional irregular wave as in Fig. 6.

In Fig. 11, the wave spectra are plotted for various locations around the WEC array for the recorded wave undisturbed by WECs (no WECs are present), diffracted wave around fixed WECs and combined diffracted and radiated wave around responding WECs. The locations considered are: (0,-5) upwave of the array, (0, 7.5) at the centre of the array, (0, 25) downwave of the array, and (15,5) at the side of the

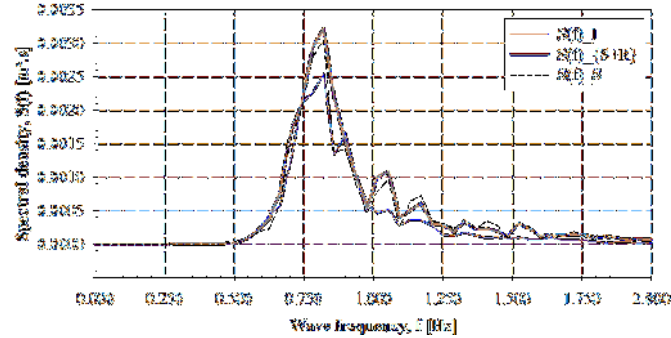
WEC column at the right. The change of H_{m0} at these locations is as shown in Fig. 10.

Specifically, spectra of undisturbed by WECs wave only, $S_I(f)$, scattered wave only, $S_S(f)$, and combined scattered and radiated wave $S_{S+R}(f)$, are presented. $S_S(f)$ appears to be very similar to $S_{S+R}(f)$, showing low impact of the radiated waves on the resulting wave spectra upwave (Fig. 11(a)). The same conclusion can be drawn for the location given at the centre of the array in Fig. 11(b). Downwave (Fig. 11(c)), scattered and undisturbed by WECs wave spectra appear to be quite similar so nearly all of the transmitted wave change is due to radiation at this certain location. At the side of the array, the wave undisturbed by WECs, combined scattered and radiated wave spectra appear to be very similar, showing limited effect of the WEC units on the resulting wave field at that location.

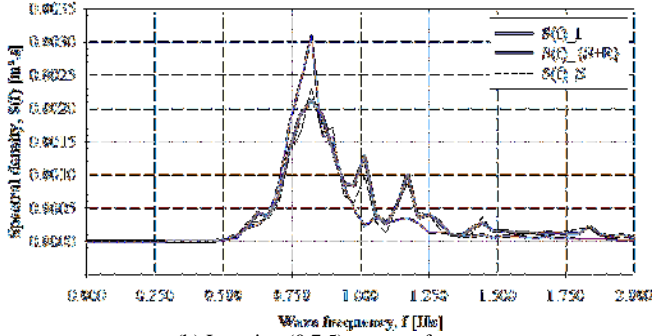


(d) Location (15,5): to side of row 1

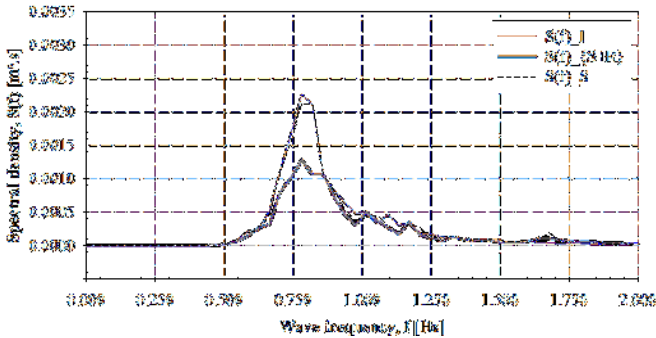
Fig. 11: Spectra of undisturbed by WECs wave only, $S_I(f)$ (thin line), scattered wave, $S_S(f)$ (dashed line), and combined scattered and radiated wave $S_{S+R}(f)$, (thick line) at locations within and around array of 5×5 floats at 5D spacing.



(a) Location (0, -5): upwave of the array
(representing frequency dependent reflection $K_R(\omega)$)



(b) Location (0,7.5): centre of array



(c) Location (0,25): downwave of array
(representing frequency dependent transmission $K_T(\omega)$)

V. DISCUSSION

In order to evaluate the capability of numerical models to predict the observed wave-field modifications either or both float response and power output are required. Response of each float has been measured. A time domain numerical model based on a state-space formulation of the hydrodynamic damping force and accounting for non-linear mechanical constraints has been shown to provide a reasonable prediction of response and power output from an individual float. These predictions depend on the magnitude of friction coefficient for the PTO and bearings and to-date have been conducted with an idealisation of the float geometry. Further analysis is ongoing to evaluate the sensitivity of mechanical friction to the assumptions associated with use of linear hydrodynamic parameters.

For the central column of floats with locations $i = 3$ and $j = 1$ to 5, total power, P_{tot} , per float is a function of the measured float velocity ($U_{3,j}$) and measured surge force ($F_{surge,3,j}$), i.e. $P_{tot,3,j} = f(U_{3,j}(t), F_{surge,3,j}(t))$. Measurements of surge force amplitude due to regular waves and due to waves radiated by an adjacent oscillating float provide the basis for evaluating linear predictions of surge force. For the other columns, with locations $i = 1, 2, 4, 5$ and $j = 1$ to 5, only float velocity, U , is measured and so surge force, F_{surge} , must be estimated to obtain total power, P_{tot} . For unidirectional waves, time variation of surge force, F_{surge} , can be estimated from those floats on the central column with the same y -ordinate. This approach neglects transverse scattering and radiation which may influence the forcing. For spread waves surge force, F_{surge} , must be either predicted numerically or an equivalent linear damping employed. The validity of the linear prediction of the surge force obtained by WAMIT is currently being assessed to calculate power output from multiple floats. An uncertainty analysis will be presented in detail in a future paper.

Regarding the wave field modifications and the effect of the WEC array configurations on the wave field, the measured change of the wave field is presented separately for the scattered waves and for the radiated waves for unidirectional irregular waves. The radiated wave is calculated as the difference between the measured total wave field and the

scattered wave field, thus it includes radiated waves that are subsequently scattered, and it also accounts for the absorption effects at the WECs. For quantifying the effect of the wave diffraction and of the radiation due to the presence of 25 WECs, on the recorded undisturbed wave field difference percentages ($\times 100\%$) are used.

For an array of 25 floats and unidirectional waves of $T_p = 1.26$ s and $H_{m0} = 0.104$ m, up to 5.1 % of wave height decrease downwave and 26.2% wave height increase upwave is observed when the 25 WECs are held stationary at mean draft, d_{buoy} . These percentages differ slightly when the recorded scattered wave heights are normalized by the target wave field (5.38 % of wave height decrease downwave and 24.0% wave height increase upwave, respectively). When looking at the effect of the WECs on the wave field due to radiation only, approximately 16.3% wave height decrease is observed downwave of the array, and 8.75-10.8 % increase upwave.

ACKNOWLEDGEMENTS

The WECwakes project is funded by the EU FP7 HYDRALAB IV programme (contract no. 261520), and is coordinated by Ghent University (Belgium) in a consortium of 7 European partners, including University of Manchester (UK), Aalborg University (Denmark), EDF – Laboratoire Saint Venant (France), Ecole Centrale de Nantes (France), University of Edinburgh (UK), and Queen’s University Belfast (Northern Ireland). The construction of the WEC models at the workshop of Ghent University has been funded by the Research Foundation Flanders (FWO) - Contract Number FWO-KAN-15 23 712 N.

REFERENCES

- [1] Folley, M., A. Babarit, L. O’ Boyle, B. Child, D. Forehand, K. Silverthorne, J. Spinneken, V. Stratigaki, and P. Troch. 2012. A review of numerical modeling of wave energy converter arrays, Proceedings of the 31st International Conference on Offshore Mechanics & Arctic Engineering, Rio de Janeiro, Brazil.
- [2] Li, Y., Y.-H., Yu. 2012. A synthesis of numerical methods for modeling wave energy converter-point absorbers. Renewable & Sustainable Energy Reviews, 16.6:4352-4364
- [3] Borgarino, B., A. Babarit, and P. Ferrant. 2012. Impact of wave interactions effects on energy absorption in large arrays of wave energy converters. *Ocean Engineering*, 41, 79-88.
- [4] Yu, Y.-H., Y. Li. 2013. Reynolds-Averaged Navier-Stokes simulation of the heave performance of a tow-body floating-point absorber wave energy system. *Computers & Fluids*, 73:104-114
- [5] N. Booij, I.J.G. Haagsma, L.H. Holthuijsen, A.T.M.M. Kieftenburg, R.C. Ris, A.J. van der Westhuysen, M. Zijlema, SWAN cycle III version 40.51AB User Manual, 2007.
- [6] P.A. Madsen, O.R. Sørensen, A new form of the Boussinesq equations with improved linear dispersion characteristics. Part 2: A slowly-varying Bathymetry. *Coastal Eng.* 18(1992), 183-204.
- [7] V. Venugopal, G.H. Smith, Wave climate investigation for an array of wave power devices, Proceedings of the 7th European Wave and Tidal Energy Conference (2007), Porto.
- [8] Alexandre, A., T. Stallard, and P.K. Stansby. 2009. Transformation of Wave Spectra across a Line of Wave Devices. *Proceedings of the 8th European Wave and Tidal Energy Conference*, Uppsala, Sweden
- [9] Silverthorne, K. and Folley, M. [2011]. A new numerical representation of wave energy converters in a spectral wave model. 9th European Wave and Tidal Energy Conference, Southampton, UK.
- [10] P. Troch, MILDwave – A numerical model for propagation and transformation of linear water waves. Internal Report, Department of Civil Engineering, Ghent University, (1998).
- [11] Beels, C., P. Troch, G. De Backer, M. Vantorre, and J. De Rouck. 2010. Numerical implementation & sensitivity analysis of a wave energy converter in a time-dependent mild-slope equation model, *Coastal Engineering*, Vol. 57(5), pp. 471-492.
- [12] Troch, P., C. Beels, J. De Rouck, and G. De Backer. 2010. Wake effects behind a farm of wave energy converters for irregular long-crested and short-crested waves. *Proceedings of the International Conference on Coastal Engineering*, No. 32(2010), Shanghai, China.
- [13] K. Budal, J. Falnes, A. Kyllingstad, G. Olstedal, Experiments with point absorbers in regular waves. Proceedings of the 1st Symposium on Wave Energy Utilization (1979), 253–282, Gothenburg, Sweden.
- [14] M. Vantorre, Third-order potential theory for determining the hydrodynamic forces on axisymmetric floating and submerged bodies in a forced periodic heave motion, PhD thesis, Ghent University, 1985.
- [15] L. Marquis, M. Kramer, P. Frigaard, First Power Production figures from the Wave Star Roshage Wave Energy Converter, Proceedings of the 3rd International Conference on Ocean Energy (ICOE-2010), Bilbao.
- [16] Thomas, S., Weller, S. and Stallard, T.J. Float response within an array: Numerical and experimental comparison. Proc. 2nd International Conference on Ocean Energy (ICOE), Brest, France, Oct 2008.
- [17] Weller, S.D. Stallard, T.J. and Stansby, P.K. 2010. Interaction factors for a rectangular array of heaving floats in irregular waves. *IET Renewable Power Generation*. 4(6), 628–637.
- [18] Ashton, I., L. Johanning, and B. Linfoot. 2009. Measurement of the Effect of Power Absorption in the Lee of a Wave Energy Converter, *Proceedings of the 28th International Conference on Offshore Mechanics & Arctic Engineering*, Honolulu, Hawaii, OMAE 2009, vol. OMAE2009-79793
- [19] M. Folley, T. Whittaker. Preliminary cross-validation of wave energy converter array interactions, submitted for the Proceedings of the OMAE2013 Conference, Nantes, France.
- [20] V. Stratigaki, P. Troch, T. Stallard, D. Forehand, M. Vantorre, J. P. Kofoed, A. Babarit, M. Folley, M. Benoit, Heaving wave energy converters for large-scale WEC array experiments, submitted for Renewable Energy.
- [21] T. Bjarte-Larsson, “Friction for a floating body heaving along a fixed vertical guiding strut,” in *Proc. 7th EWTEC*, Porto, Portugal, 2007.
- [22] M.S. Longuet-Higgins, D.E. Cartwright, and N.D. Smith. Observations of the directional spectrum of sea waves using motions of a floating buoy. In *Ocean Wave Spectra*, pages 111–136. Prentice Hall, New York, 1963.
- [23] Y. Goda and Y. Suzuki. Computation of refraction and diffraction of sea waves with Mitsuyasu’s directional spectrum. *Tech. Note of Port and Harbour Res. Inst.*, 230, 1975.
- [24] D. I. M. Forehand, A. P. McCabe, and A. R. Wallace, “A hydrodynamic, time-domain, wave energy converter array model using state-space techniques,” to be submitted to *Ocean Engineering*, 2013.
- [25] (2013) WAMIT version 7.0 user manual. [Online]. Available: <http://www.wamit.com/>.
- [26] K. Friedrich. Friction and wear of polymer composites, E , 1986.
- [27] Aalborg University. (2007): WaveLab 3.33 Manual. homepage: <http://www.hydrosoft.civil.auc.dk/>